Spatiotemporal coordination of the cell divison cycle

Thibeau Wouters

Under the supervision of Lendert Gelens and Daniel Ruiz Reynés

December 27, 2021

Abstract

In oscillatory media, regions oscillating faster than their surroundings, as well as topological defects, can act as sources of waves which end up synchronizing the whole medium. The former give rise to target patterns, while the latter develop into spiral patterns. In biological systems, these waves are a crucial way of transmitting information efficiently. While target patterns have been studied in detail before, specifically in the context of biology, our interest in spiral wave phenomena is inspired by recent observations of such structures in cell cycle oscillations of *Xenopus laevis* frogs. In order to understand how wavespeed, and the speed by which these patterns entrain the whole system, depend on the properties of the underlying limit cycle and details of the system, we rely on numerical simulations. In this research internship, we take this approach in order to understand how variations in the system's parameters affect these speeds and compare them between target and spiral patterns in two-dimensional systems, and also investigate the interaction between the two competing structures of target patterns and spiral waves when present in the same system.

Contents

1 Introduction

Oscillations are present everywhere in Nature, from the orbits of planets and stars on cosmic scales, to cycles in the divison of cells in biological systems. Organisms rely on travelling wave phenomena and pattern formation to transmit information across large distances in an efficient way. Spiral waves and target wave patterns are particular examples of dynamical pattern formation appearing in complex spatiotemporal systems and have been observed in physical, chemical and biological contexts, such as the famous Belousov-Zhabotinsky (BZ) reaction [1–3], the catalytic oxidation of CO on a Pt(110) surface [4], the electrical activity of cardiac muscles [5], the release of free intracellular calcium Ca^{2+} in *Xenopus laevis* oocyte [6] and cAMP waves during the aggregation phase of *Dictyostelium discoideum* amoebae [7, 8].

Travelling waves have been observed before by the team of *Dynamics in Biological systems* (DiBS)[1], who supervised this research internship, in the *Xenopus laevis* frog's cell extracts. Since these waves and patterns play an important role in the coordination of the cell cycle oscillations, a lot of research has been dedicated to understanding these patterns, their properties and their origin through mathematical models which can be studied numerically. In particular, in Refs. [9–12], experiments have inspired numerical work on the modelling of cell cycle oscillations in one-dimensional systems in order to understand observations from experiments.

Recently, the DiBS team observed spiral patterns for the first time in their experiments. The spirals appeared together with target patterns in *droplets* containing extract, which are two-dimensional extended spatial systems. A snapshot, showing several spiral and target waves, is shown in Figure A.12. Motivated by this observation, we would like to model the formation of target patterns and spirals in two-dimensional systems in order to understand their properties, such as speeds of the waves spreading out and the speed by which these patterns entrain the medium, as a function of the model's parameters and details of the system. Given the observation that target and spiral patterns can appear simultaneously in a system, we also study the interaction between these patterns, again as a function of parameters underlying the model of the oscillations.

The report is organized as follows. In Section 2, we introduce the model used to study the wave phenomena and highlight important points in our computational algorithms. Section 3 then provides some conclusions drawn from the numerical studies, based on the results provided in the appendices. Section 4 briefly discusses estimates of wave speeds and periods as observed in experiments and how they relate to the numerical studies. Finally, an outlook for future work is provided in Section 5.

[1]The DiBS is part of the *Department of Cellular and Molecular Medicine* and is situated at Gasthuisberg, Leuven. More information about their research can be found on their website.

2 Methods

In this section, we provide detailed information on how we numerically study pattern formation and properties of target patterns and spiral wave phenomena. First, we introduce the set of equations used to model the oscillations. Then, we briefly explain the numerical methods used to compute wave and envelope speeds. Finally, we clarify how we numerically study the interaction between target patterns and spirals.

2.1 The Fitzhugh-Nagumo equations

Whenever we want to model a complicated, biological system, we necessarily have to make a compromise between simplicity, ensuring that our analysis is tractable and solvable, and complexity that is inherently present in the system due to many biochemical interactions. Here, we employ a system of partial differential equations of two variables u and v which are capable to capture the main behaviour of target and spiral patterns. For our model, we take inspiration from earlier work of the DiBS lab on travelling waves in one spatial dimension [10].

To model the cell cycle oscillations, we make use of FitzHugh-Nagumo (FHN) equations [13, 14] related to the well-known Van der Pol oscillator [15]. The equations are

$$\partial_t u = \varepsilon^{-1}\left(v - \tfrac{1}{4}du(u^2 - b)\right) + D_u\nabla^2 u \equiv \varepsilon^{-1}\left(v - f(u)\right) + D_u\nabla^2 u \tag{2.1}$$

$$\partial_t v = a - u + D_v\nabla^2 v\,. \tag{2.2}$$

Due to the different nature of the terms, the above equations are called *reaction-diffusion* (RD) equations. The variables u and v represent chemical concentrations or activity, and both are allowed to diffuse in space. The variable u is said to be an *inhibitor*, while v is an *activator*, due to the signs of terms on the right hand sides. We mostly study wave phenomena in two dimensions, such that $\nabla^2 = \partial_x^2 + \partial_y^2$.

The reaction part of the above equations has a unique fixed point, the homogeneous steady state solution (HSS), given by

$$(u_{\mathrm{HSS}}, v_{\mathrm{HSS}}) = \left(a, \tfrac{d}{4}a(a^2 - b)\right) \tag{2.3}$$

The system is in the oscillatory regime if $|a| \leq \sqrt{b/3}$, while the system can be excitable for other values of a. Here, however, we will limit ourselves to values of a such that the system is in the oscillatory regime.

Let us briefly discuss how the various parameters of the above RD equations influence the dynamics of solutions. The parameter ε is called the *timescale separation* between the variables u and v. Essentially, ε determines the shape of the time series of u and v: for

low values of ε, the oscillations are relaxation-like, while for high values of ε, the oscillations have sinusoidal waveforms for both variables. An example of this is shown in Figure A.1(c) and Figure A.1(d). The parameters b and d, on the other hand, determine the shape of the cubic nullcline[2], as indicated in Figure A.1(b). However, a suitable rescaling of the variables allows us to absorb these parameters in ε and a. Indeed, starting from equations (2.1) and (2.2) and performing the change of variables

$$\tilde{u} = \frac{2}{\sqrt{b}}u, \quad \tilde{v} = \frac{8}{b\sqrt{b}d}v, \quad \tilde{t} = \frac{4}{db}t, \quad \tilde{x} = \frac{2}{\sqrt{db}}x, \quad \tilde{y} = \frac{2}{\sqrt{db}}y\,. \tag{2.4}$$

One can easily show that the system of equations then becomes

$$\partial_{\tilde{t}}\tilde{u} = \tilde{\varepsilon}^{-1}\left(\tilde{v} - \tfrac{1}{4}\tilde{u}(\tilde{u}^2 - 4)\right) + D_u\tilde{\nabla}^2\tilde{u} \tag{2.5}$$

$$\partial_{\tilde{t}}\tilde{v} = \tilde{a} - \tilde{u} + D_v\tilde{\nabla}^2\tilde{v}\,, \tag{2.6}$$

where

$$\tilde{\varepsilon} = \frac{16}{(db)^2}\varepsilon, \quad \tilde{a} = \frac{2}{\sqrt{b}}a\,. \tag{2.7}$$

Therefore, we take $d = 1$ and $b = 4$ fixed from now on. Finally, the parameter a affects the vertical nullcline and determines the HSS, as is clear because of equation (2.3) and the plot of the nullclines. Consequently, it determines the equilibrium point of the oscillations for u and v, since d and b remain fixed. For this reason, we also call a the *asymmetry parameter*. Default parameter values in simulations are $a = 0, \varepsilon = 0.1, D_u = 1$ and $D_v = 0.1$.

The above FHN equations are simulated in a square domain with sides of length $L = 200$. The equations are numerically integrated using the forward Euler scheme in *Python* where the domain is subdivided into N^2 grid points, with $N = 200$, using no-flux boundary conditions and for a time $T = 1000$ with Euler time step $\mathrm{d}t = 0.01$. In case ε is smaller than 0.1, the space-time discretization is improved, depending on the value of ε, because of sharp 'jumps' in the time series which require more care in the numerical calculations. The u and v values are saved after a certain amount s of Euler steps, such that $\Delta t \equiv s\,\mathrm{d}t = 0.01$, independent of the discretization.

The choice of the initial condition (IC) depends on which pattern we want to study. To generate target patterns, we choose a homogeneous IC for both u and v: $u_0(x, y) = 1$, $v_0(x, y) = 0$. A target pattern emerges if the system contains a *pacemaker*, which is a region in space which oscillates faster than its surrounding medium. We denote the period inside the pacemaker region as P_i, while the period outside the pacemaker region is denoted by P_o, with $P_i < P_o$. In our 2D simulations, the pacemaker region will be a circle of radius R and centre $(\frac{L}{2}, \frac{L}{2})$. Default values are $R = 20$, $P_o = 10$ and $P_i = 9.5$. We also define $h \equiv P_o - P_i$, the period difference between the pacemaker region and the surrounding medium. Numerically,

[2]The *nullclines* are defined as the curves in the (u, v) plane satisfying $\partial_t u = 0$ or $\partial_t v = 0$ in absence of diffusion. The first equation gives the curve $v = f(u)$, referred to as the cubic nullcline, while the second equation gives $u = a$, a vertical line. The intersection of the nullclines is the HSS.

we can create such a pacemaker region by rescaling dt at each time step with a *scale factor* which depends on space to fix the periods to their desired values.[3].

To study spirals, on the other hand, we employ an initial condition which contains a *topological defect* [16–18], namely

$$u_0(x,y) = \frac{(x-x_0)}{L}, \quad v_0(x,y) = \frac{(y-y_0)}{L}\,, \tag{2.8}$$

which has a phase singularity located at (x_0, y_0) for $a = 0$. The location of the spiral tip depends on the HSS, and hence changes only if we vary a. We take $x_0 = y_0 = \frac{L}{2}$, such that the topological defect is located at the centre of the system for $a = 0$. From now on, we will use x^* and y^* to denote the coordinates of the centre of the pattern of interest. For target patterns, this will always be $(x^*, y^*) = \left(\frac{L}{2}, \frac{L}{2}\right)$, the centre of the pacemaker. For spirals, this will denote the location of the spiral tip. From the u, v data of simulations, we can locate the spiral tip via code inspired by the framework to detect phase defects from [19].

2.2 Wave speed and envelope speed calculations

Once the FHN equations are numerically integrated as explained above, the solution $u(t; x, y)$, $v(t; x, y)$ is a target pattern or a spiral, depending on our choice of initial condition: examples are shown in Figure A.2. We are interested in properties of the pattern and how they affect the surrounding medium. For this, we follow the principles and ideas of earlier work from the DiBS lab [10], which are briefly summarized below. We take a slice of the solution by fixing the y-coordinate and define $U \equiv u(t; x, y^*)$ and $V \equiv v(t; x, y^*)$. U and V can be visualised by a *space-time* plot, as given in Figure A.3. From the U (or V) data, we then identify the (t, x) coordinates where U (or V) crosses zero from below. These points are then grouped together in different *profiles*, shown in black in Figure A.3. For practical reasons, we construct profiles starting from $x = 0$, respectively $x = L$, if $x^* > \frac{L}{2}$, respectively $x^* < \frac{L}{2}$, until we reach $x = x^*$.

These profiles represent waves travelling outwards from the pattern towards the surrounding medium. Its wave speed can be determined as follows. Each profile consists of a rather flat part around the borders of the system, and a valley reaching all the way until the centre of the pattern. By choosing a profile and considering its (x, t) coordinates, we can fit a straight line through a section of the valley-shaped part of the profile. The slope of this straight line is then the wave speed. From the profiles, we can also construct the *envelope* of the wave as follows. For each profile, we define the *envelope point* to be the transition point from the valley-shaped section to the flat section of the profile. The envelope is then simply the set of all envelope points and can be fitted using a function of the form $x = D + Ct^\gamma$.

[3]For this, we need to know the period of the solution P in case no time rescaling is performed. This can be computed easily be 'turning diffusion off' (setting $D_u = D_v = 0$) and solving the FHN equations.

The *envelope speed* is defined to be the parameter C. However, in most cases, the envelope does *not* spread out linearly during an initial transient time period, which means that γ is significantly different from one, and the parameter C cannot be properly interpreted as a speed. Therefore, we also perform a linear fit through the second half of the envelope points, and return the slope C_l as envelope speed, which we will refer to as *linear envelope speed*.

A relation between the wave and envelope speed was derived analytically and checked numerically for 1D target patterns in [10]. The relation is

$$C = \frac{P_o - P_c}{P_o}\, c\,, \tag{2.9}$$

where P_c is the period at the 'centre' of the system, *i.e.* the period at (x^*, y^*). In simulations, P_c can easily be inferred from the time series $u(t; x^*, y^*)$ or $v(t; x^*, y^*)$. This relation was also checked for 2D target patterns and spirals.

We are interested in the dependence of the wave-and envelope speeds of target as well as spiral patterns, as a function of the parameters of the FHN equations. For this, we perform *parameter sweeps*, where we vary a single parameter over a certain range, and for each value perform a simulation as detailed above and 'measure' the speeds at the end. This is a daunting computational task, and therefore, the code is adapted to run on a cluster of supercomputers.

2.3 Competition between spirals and target patterns

As touched upon earlier, we are interested in the interaction between target patterns and spirals. For this, we study the 'competition' between spirals and target patterns when both are present at the same time in the system. For this, we again use the cross-gradient IC given in equations (2.8), but this time, we put the topological defect at $(x_S, y_S) = \left(\frac{3L}{4}, \frac{L}{2}\right)$. At the same time, we define a circular pacemaker with centre at $(x_T, y_T) = \left(\frac{L}{4}, \frac{L}{2}\right)$. The FHN equations are then integrated for a time $T = 1000$. Afterwards, we try to detect a phase singularity in the data. If none is detected, or if its location has moved significantly compared to the initial spiral tip location (x_S, y_S), then we decide the pacemaker has 'won', *i.e.* has entrained the entire medium. If the spiral is still present and its tip is still close to (x_S, y_S), then we detect if the pacemaker region is still present or not. If so, then we have a 'draw' and both the target and the spiral pattern are still present. Otherwise, the spiral has 'won' and has taken over the entire system.

3 Results and discussion

We now discuss important conclusions from our simulations. The results of the simulations are provided with plots in the appendices. First we discuss the speeds of both patterns in two dimensions and compare our observations with earlier work focusing on target patterns in one dimension. Next, we analyse the interaction between target patterns and spirals.

3.1 Speeds of target patterns and spirals

The speeds of target patterns and spirals is studied via parameter sweeps, as described above. First, we focus on target patterns, and vary R, the radius of the circular pacemaker, and h, the period difference between the pacemaker region and the surrounding medium. Then, we study both target patterns and spirals at the same time as we vary a, ε and the diffusion coefficients.

When increasing the size of the pacemaker (by varying R), the wave speed decreases and the envelope speed increases as shown in Figure A.4. For very large R, both speeds asymptote towards a constant. When we increase the period difference h, again the wave speed decreases and the envelope speed increases: see Figure A.5. However, both do not seem to asymptote towards a constant. This qualitatively agrees with the simulations in 1D from [10][4].

When we increase the asymmetry parameter a, the speeds are only weakly influenced as can be seen in Figure A.6. This again agrees with the results in 1D. The wave speed of spiral waves is not influenced at all by the variation of a: these wave speeds vary between 2.3606 and 2.3726, and a linear fit through the (a, c) points of spiral waves has a very small slope of 0.00682 (with a p-value of the fit around 10^{-6}).

When varying the diffusion coefficients, we mimic the approach from [10]: in one sweep we vary D_u and put $D_v = D_u$, in another sweep we vary D_u and fix $D_v = 0$. Here, it is most interesting to focus on the wave speeds of the patterns. The results, after normalizing the speeds to their values at $D_u = 1$, are shown in Figure A.7 (a) and (b), along with the approximation $c \approx \sqrt{D_u}$. The wave speeds of spirals is in both cases well-approximated by the $\sqrt{D_u}$ approximation. The same can be said about wave speeds of target patterns in the second sweep, where $D_v = 0$, but *not* in the first case, where $D_v = D_u$. Here, the behaviour of the wave speed as a function of D_u is different from the 1D case.

In order to compare the wave speeds of target patterns between one and two dimensions,

[4] In [10], h is defined slightly differently as $h = (P_o - P_i)/P_o$, such that our h is ten times larger using the default value $P_o = 10$. Also note that our choice of 'default' parameter values is different from [10], so we do not expect a quantitative agreement with the reference. Our simulations show that the speeds in 1D and 2D are the same for the same set of parameter values, if the pacemakers are large and ε is small.

we performed a parameter sweep over the same D_u range for one-dimensional pacemaker-driven systems and compared the wave speeds and periods at the centre. The result is given in Figure A.8. The fact that wave speeds of target patterns are larger in 2D can be attributed to the influence of an increased amount of diffusion on the period of the waves, due to the fact that we are in two spatial dimensions rather than one. Indeed, the dispersion relation tells us that waves with a larger temporal period have larger wave speeds [10]. The surrounding medium has a larger effect on the period in 2D and increases the period, thereby increasing the speeds. This effect is precisely what causes the deviation from the $\sqrt{D_u}$ approximation (shown as a black dashed curve in Figures A.7 and A.8), which is valid for travelling waves in the medium without inhomogeneities (such as pacemaker regions). Note that in the sweep with $D_v = 0$, the influence of diffusion on the period is much smaller compared to the sweep with $D_v = D_u$. Therefore, in the former sweep, the speeds are closer to the $c \approx \sqrt{D_u}$ approximation.

Finally, we study the effect of varying the time-scale separation ε on the wave- and envelope speeds of both wave patterns: the result is given in Figure A.9. Here, target and spiral waves have quite a different response on increasing ε. Whereas the wave speed of target patterns decreases, the wave speed of spiral waves increases. The envelope speeds of both patterns decrease, but the target patterns are more stable against this variation compared to spirals. An interesting consequence, which we will use again in Section 3.2 below, is that from $\varepsilon \geq 0.15$, target patterns have a larger envelope speed than spirals, while for $\varepsilon \leq 0.15$, the spirals have a larger envelope speed.

We also compared the approximation of the envelope speed as given in equation (2.9) in each parameter sweep, and found that the relation still holds in 2D for target patterns as well as for spirals.

3.2 Competition between spirals and target patterns

As already explained above, we are also interested in the competition between spirals and target patterns when both are present in the system. We want to know which of the two patterns survives in the end, and how this depends on the choice of parameters. For this, we study two cases.

First, we vary parameters specific to the pacemaker: R and h. The results of the simulations are shown in Figure A.10. On the left hand side of this figure, we show the outcome of the competition between the two patterns for each (R, h) pair, with blue, respectively yellow, denoting the scenario where only the target, respectively the spiral, was observed in the end, and gray denoting a draw, *i.e.* both the target and the spiral were present at the end. We immediately see that the most important property to decide the outcome of the competition is the period difference h. Indeed, we identify three horizontal 'bands': low values of h mean the spiral will win, intermediate values result in a draw, while for high h,

the pacemaker is guaranteed to dominate. The influence of varying R is unimportant except close to transitions between these various bands.

In a second case, we vary ε and h, such that the variation of one of the parameters also influences the properties of the spiral. The result is shown in Figure A.11 on the left. We no longer can identify different horizontal bands, which implies that the variation of ε has a more complicated influence on the competition. Nevertheless, we can still draw the same conclusion about the influence of h: a faster pacemaker (*i.e.*, a larger period difference with the environment) has more chance to survive the interaction with the spiral or win.

After this investigation, we also tried to pin down which property of the patterns is the deciding factor in the competition. One can expect that the envelope of the patterns is important, since the interaction occurs away from the sources of the patterns. This idea is tested in a more quantitative way as follows. We perform parameter sweeps, as described earlier in Section 2.2, over the same pairs of variables as shown in Figure A.10 and Figure A.11, with either only a spiral or a target pattern present in the system, and measure the same set of observables as discussed above. We consider the difference between the envelope speed of the spiral and the envelope speed of the target $C_S - C_T$ and group the differences according to the outcome of the competition for each pair of parameters. Each set of differences in envelope speed is then visualized via a boxplot, shown in Figure A.10 and Figure A.11 on the right hand sides. The analysis shows that the difference in envelope speed $C_S - C_T$, when ignoring outliers, is negative in case the target won in the end, lies around zero in the case a draw was reported, and is positive in the case that the spiral has entrained the entire medium. This seems to indicate that the pattern with the highest envelope speed will in the end dominate the system.

In earlier work, the DiBS lab studied the competition between two pacemakers in one-dimensional systems [11]. Figure 3(c) in Ref. [11] shows that larger or faster (higher period difference with the surrounding medium) pacemakers in the end take over the medium. From our investigations, or from the figures in [10], we see that larger and faster pacemakers have a higher envelope speed. This agrees with our observation established above that the envelope speed of patterns seems to be the deciding factor in the competition for entraining the system.

4 Speed and period estimates from experiments

The main motivation to study the properties of spiral waves in RD systems was the observation of such spirals in *Xenopus laevis* extracts: recall Figure A.12. We can now make the connection between the numerical simulations and the experimental data. Via some elementary data processing in *Python*, we are able to extract a few rough estimates of wave speeds and periods of the target and spiral waves. Wave speeds can be estimated from the distance

travelled by a wave from the locations of wave fronts between different snapshots of the experiment and dividing this distance by the separation in time. Periods can be estimated by obtaining the time series at a specific location and, through Fourier transforms, get an indication of the frequency of the oscillation.

We find that wave speeds of target patterns and spiral waves are roughly identical to each other: we estimate the wave speed of target patterns to be around $(0.409 \pm 0.018)\mu$m/s, while the wave speed of spirals is around $(0.417 \pm 0.080)\mu$m/s. The period of the oscillations, on the other hand, is drastically different. Periods measured in experiments where spiral patterns are observed, is on the order of 10 to 15 minutes, while earlier experiments, which did *not* have spiral waves in the system but only target patterns, were always consistent with periods on the order of 30 to 40 minutes [12]. The discrepancy is likely due to the fact that pacemakers, by their very definition, keep the period of oscillations in a specified range (*i.e.* between P_i and P_o in the notation from Section 2.1), while in the presence of spiral waves, the period of the oscillations is not restricted. This is also clear from Figure A.7(d), showing that the period in a system with spiral waves can be much lower compared to a system with only target patterns.

5 Outlook and conclusion

Science is a rigorous, methodological way of exponentially increasing the number of unanswered questions by answering questions. The work related to this internship is no exception. Here we briefly propose possible topics to be explored in future work, inspired by the results presented above.

An elementary question, which unfortunately is hard to explore in numerical simulations, is what exactly triggers the creation of spiral waves in cell cycle oscillations. Our simulations start from a topological defect, without any prior event possibly causing the creation of such defects. It seems plausible, from experimental footage, that the merger of droplets of extracts could provide a disruption in the system which initiates the spiraling motion, but due to the limited amount of observations, this is hard to test quantitatively. Once the production mechanism of spirals is understood from a modelling point of view, and we know how to trigger spiral waves, we can bridge the gap between simulations and actual experiments on biological systems.

A next step is then to identify which of the parameters of the system, or more concretely the effect due to their variation on the dynamics, is the most essential in understanding the observed speeds and periods in the experiments. Recently, the DiBS lab hired a new PhD student whose first goal is to find out which equations are most fit to model the experiment, using machine learning. The experimental observation of spiral waves inspired this research internship. It is hoped that the results from this internship and future work, combined

with machine learning methods, will be able to inspire future experiments on spiral wave phenomena in *Xenopus laevis* cells.

In this work, we studied the interaction between target patterns and spiral waves and established that envelope speed is an important factor in entraining a system. In future work, one can check this 'conjecture' in other parameter sweeps, or repeat the analysis with the competition between two pacemakers in 2D (extending the work from [11]) or two spirals, instead of one target and one spiral.

One can also think about scenarios where pacemaker regions and topological defects come closer to each other in space, and how this would affect their interaction, with an extreme case being a spiral tip located inside a pacemaker region. In fact, there is a strong motivation to study such scenarios in future work. In the experiments, we observed a spiral wave "turn into" a target pattern after a few oscillations. Considering that we are dealing with biological systems rather than idealized simulations, we might have to drop the assumption, implicitly used in this work, that parameters are constant in space and time to recreate this observation in simulations. Numerical explorations show that through varying a, we can start a simulation with a spiral and end up with a target pattern. However, this requires us to make the system excitable, and we would like to find other ways which are more suitable.

Finally, we also repeat the observation, coming from the simulations as well as the experimental data, that periods of oscillations are much lower if spirals are present, which could be the main reason why it appears in cell divison cycles. This surprising discovery can be investigated further by studying how the period depends on the set-up of the system (*e.g.* multiple spirals or pacemakers).

To conclude, in the research internship, we have looked at the properties of spiral waves and target patterns in two-dimensional systems by numerical studies of a FitzHugh-Nagumo model of RD equations. The similarities or differences between how these two patterns behave under variation of the parameters of the system can provide crucial information regarding how biological systems rely on either target patterns or spiral waves (or both) to transmit information within the cytoplasm of a cell. Future work can build on the interaction and relation between the two patterns, and study in detail how the numerical simulations are related to experiments performed in the lab, possibly even inspiring future experimental work in the field.

Understanding how waves, originating from pacemaker regions or topological defects, travel around in biological systems is of central importance in understanding how life organizes and coordinates oscillations in basic functions such as divisions in cell cycles. With evolution as driving force and vast amounts of time, lifeforms were able to construct mechanisms that optimize their functioning. Figuring out the properties of different wave patterns appearing in Nature is a crucial step towards understanding why evolution curated these distinct mechanisms to transmit information, eventually adding to our understanding of deeper questions about life in general.

A Appendix

A.1 Methods and algorithms

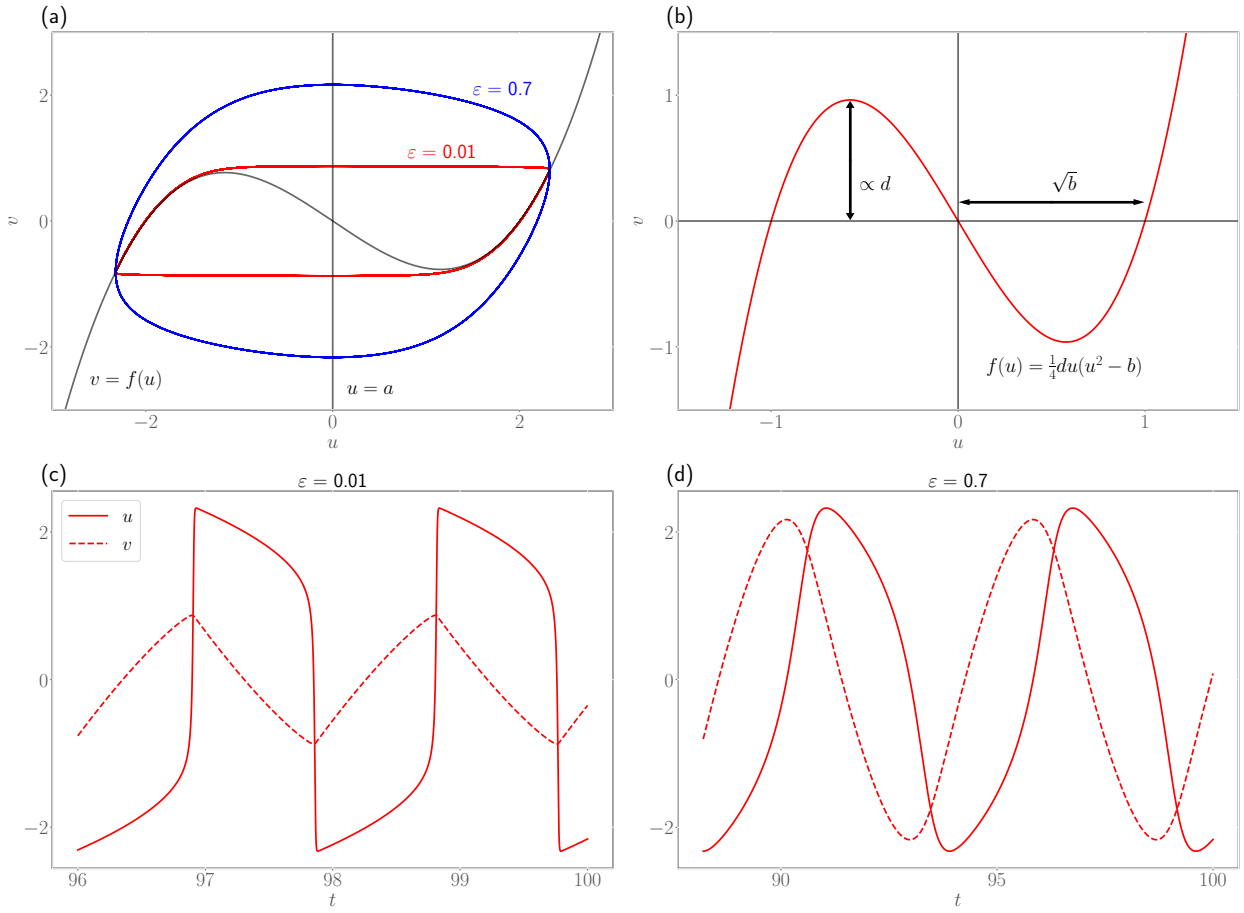

Figure A.1: (a) Examples of two limit cycles of the FHN model from equations (2.1, 2.2) with $a = 0$, $b = 4$ and $d = 1$ for two different values of ε: $\varepsilon = 0.01$ (red) and $\varepsilon = 0.7$ (blue). Nullclines are shown in gray. (b) Plot of the cubic nullcline $f(u)$, showing the effect of the parameters b and d on its shape. (c) Time series for u and v of the limit cycle with $\varepsilon = 0.01$. (d) Time series for u and v of the limit cycle with $\varepsilon = 0.7$.

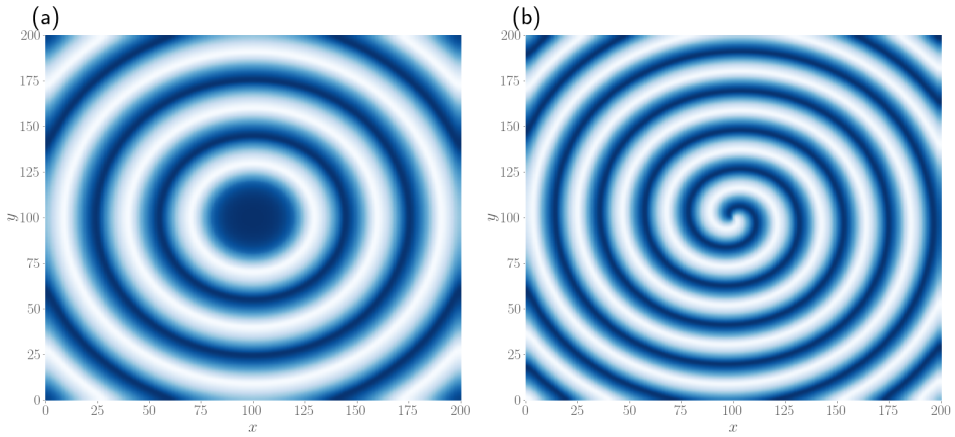

Figure A.2: (a) Example of a target pattern arising when integrating the FHN equations with a circular pacemaker region, with radius $R = 20$, at the centre of the system. (b) Example of a spiral arising when integrating the FHN equations with a topological defect at the centre of the system. Parameter values are at their default values discussed in the text. Blue and white denote positive and negative values of u, respectively.

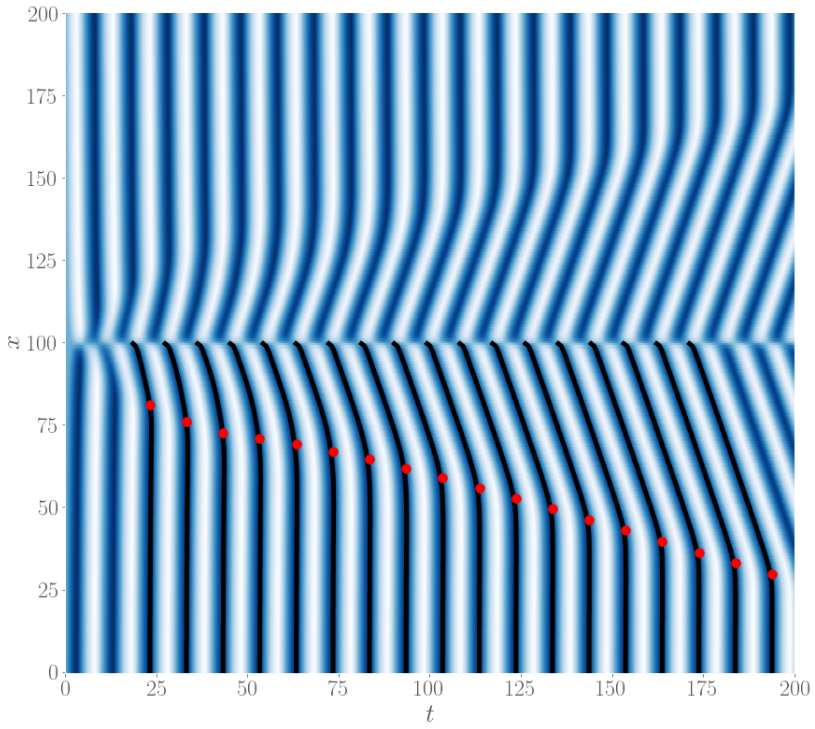

Figure A.3: Example of a space-time plot of the U values, where U is defined in Section 2.2, in a simulation of a spiral pattern. The spiral tip is located at the centre of the system. Shown in black are the profiles detected by our algorithm, from which the envelope points, shown in red, are found. Parameter values are at their default values discussed in the text. Blue and white denote positive and negative values of U, respectively.

A.2 Results of parameter sweeps

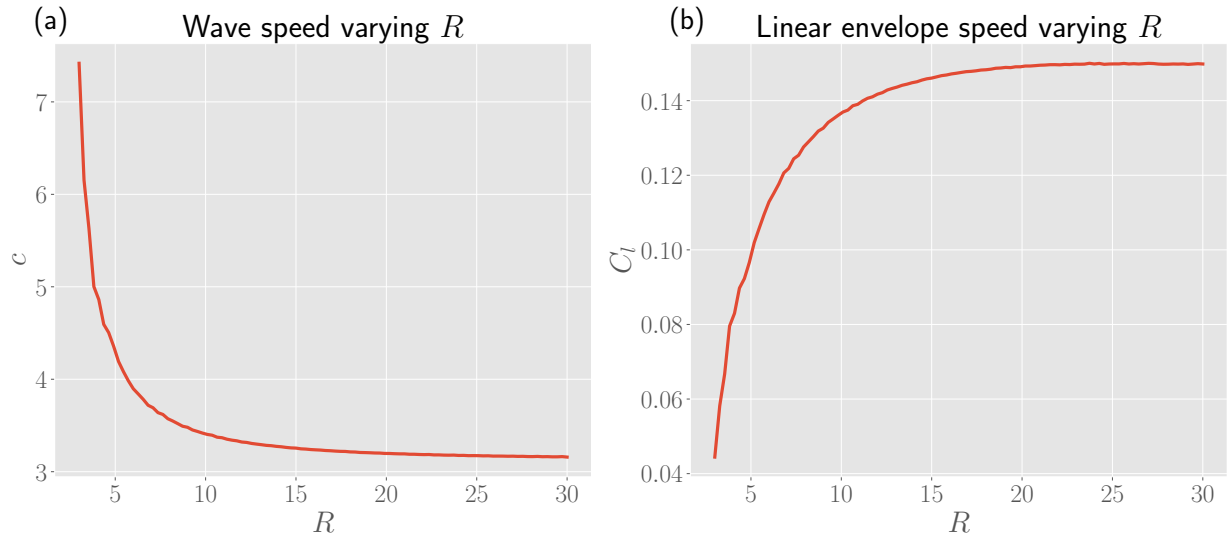

Figure A.4: Wave speed and linear envelope speed for varying R, the radius of the circular pacemaker region.

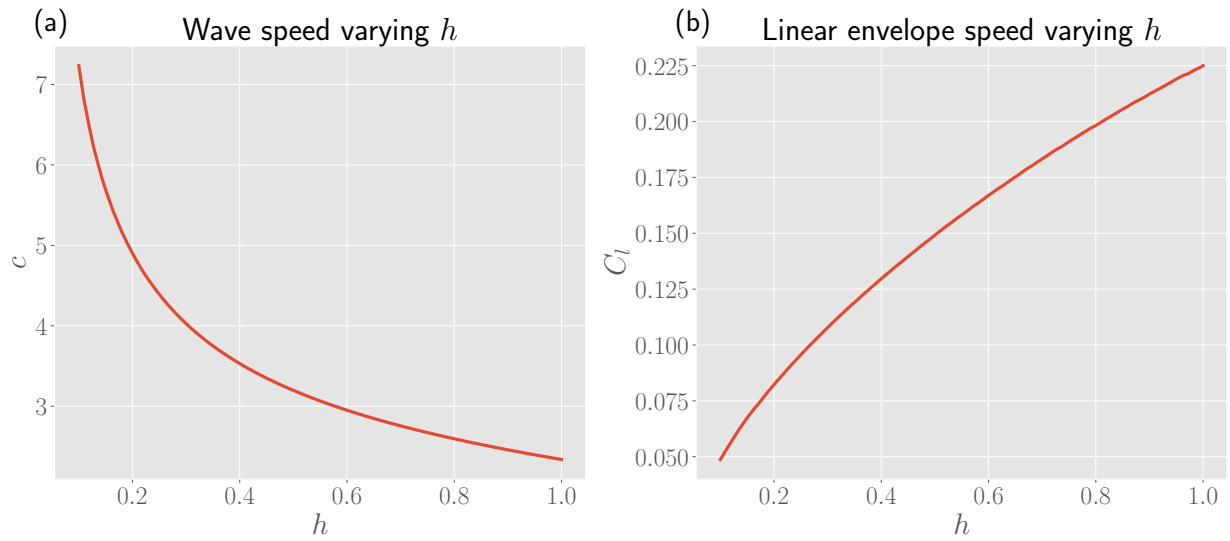

Figure A.5: Wave speed and linear envelope speed for varying h, the period difference between the pacemaker region and the surrounding medium.

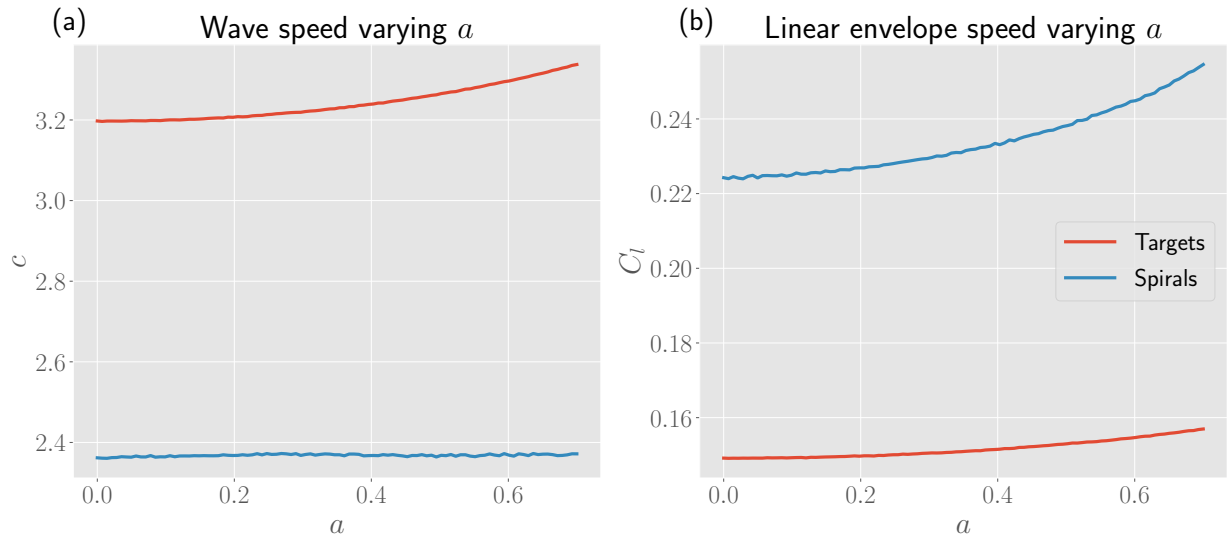

Figure A.6: Wave speed and linear envelope speed for varying a, the asymmetry parameter.

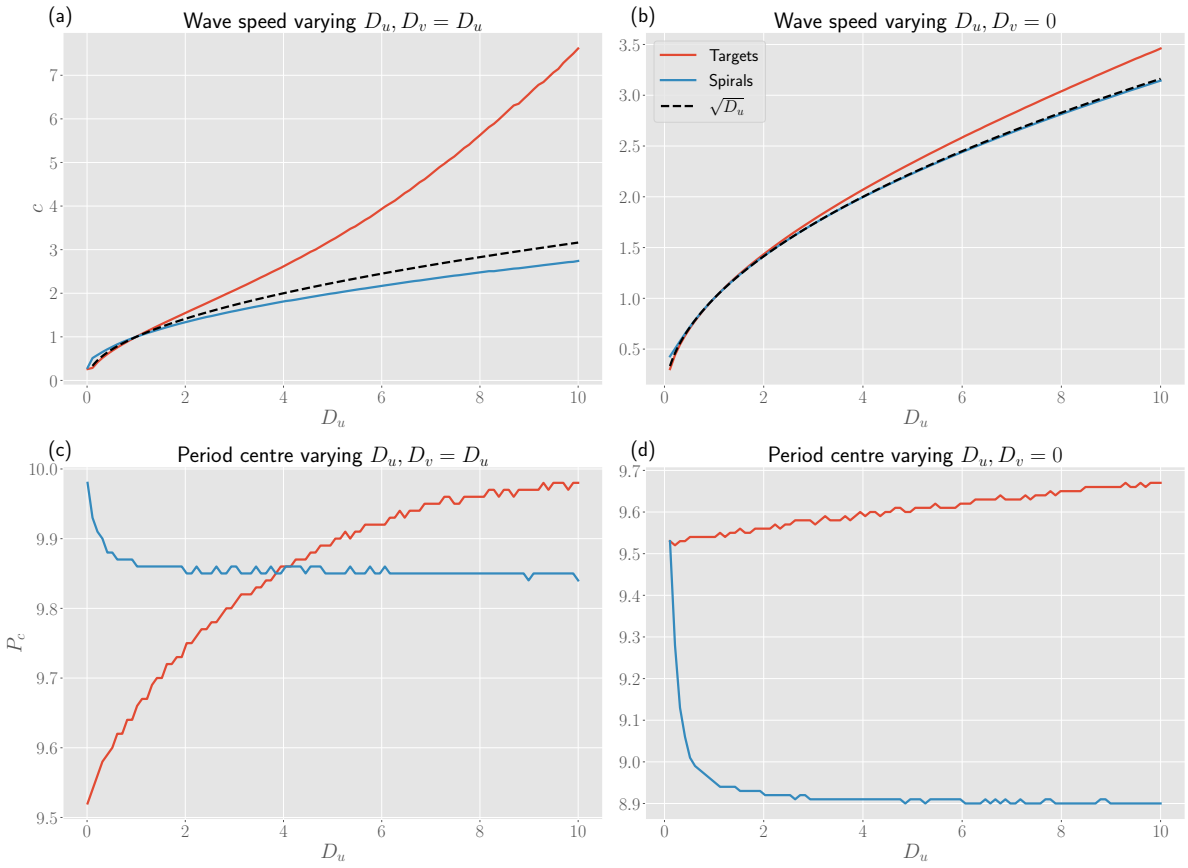

Figure A.7: Wave speeds and periods of oscillations at the centre (x^*, y^*) for varying D_u. Panels (a) and (c) have $D_v = D_u$, while panels (b) and (d) have $D_v = 0$.

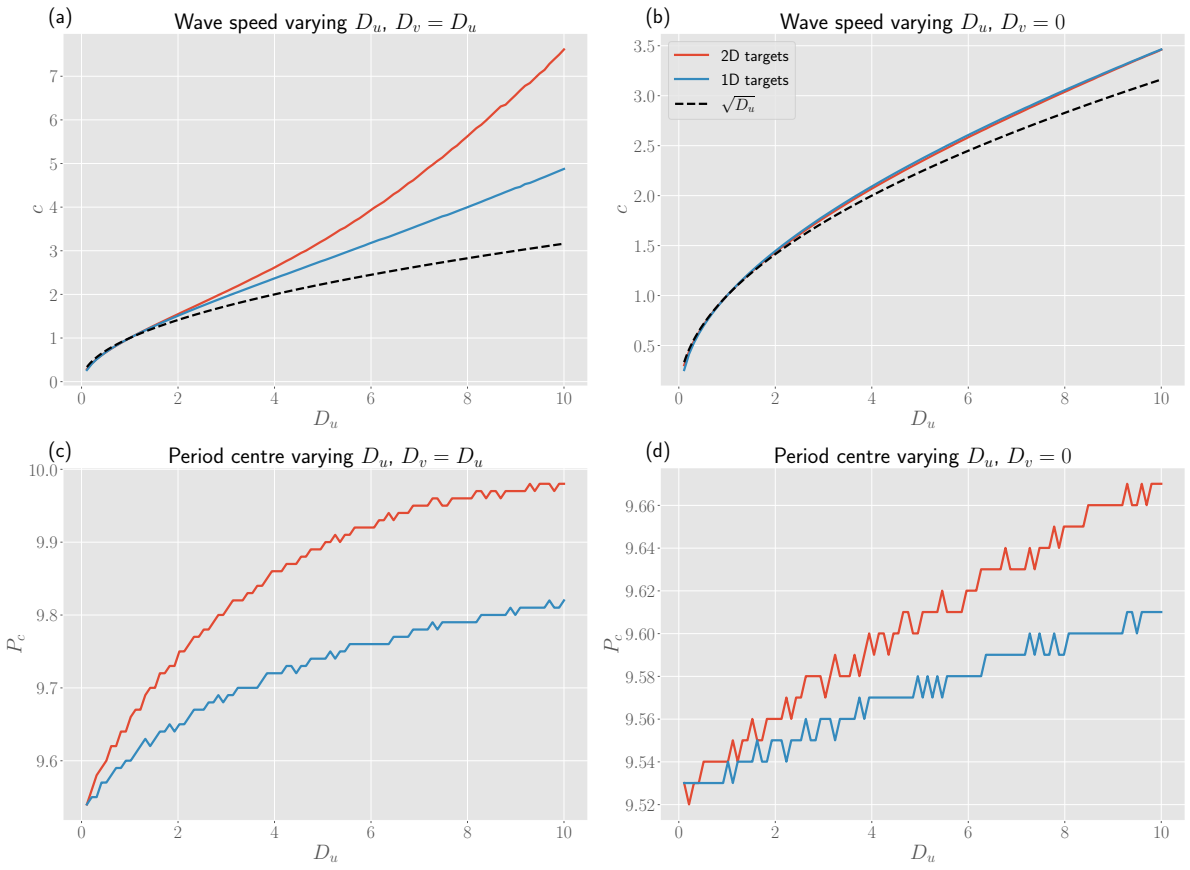

Figure A.8: Wave speeds and periods of oscillations at the centre (x^*, y^*), respectively $x = L/2$, of target patterns in 2D, respectively 1D, for varying D_u. Panels (a) and (c) have $D_v = D_u$, while panels (b) and (d) have $D_v = 0$.

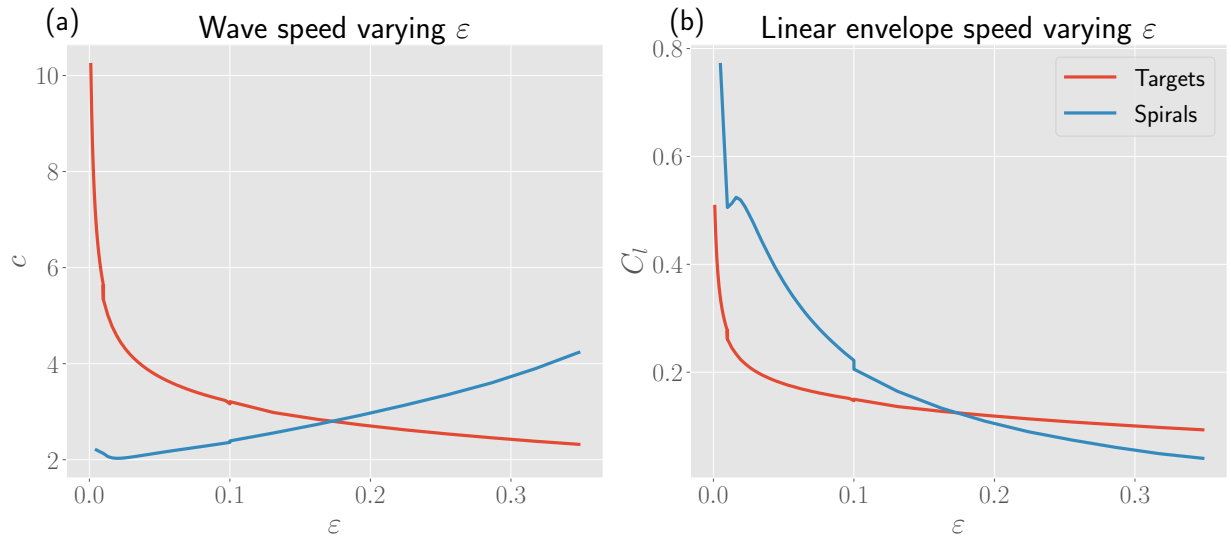

Figure A.9: Wave speed, linear envelope speed and period at the centre for varying ε, the time-scale separation.

A.3 Results of competition

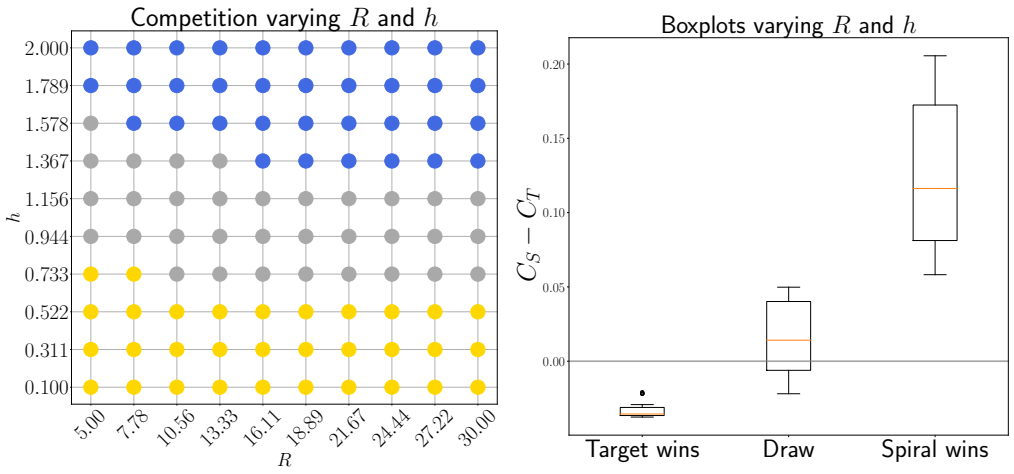

Figure A.10: Competition between spirals and target patterns while varying R and h of the pacemaker. *Left:* Result of the competition while varying R and h. The colour of each (R, h) dot denotes the outcome of the simulation for that pair of parameters: yellow if the spiral has won, gray if both the spiral and target pattern remain (draw), and blue if the target has won. *Right:* Boxplots of the difference in envelope speed of the spirals C_S and the target patterns C_T at all pairs (R, h), grouped according to the outcome of the competition.

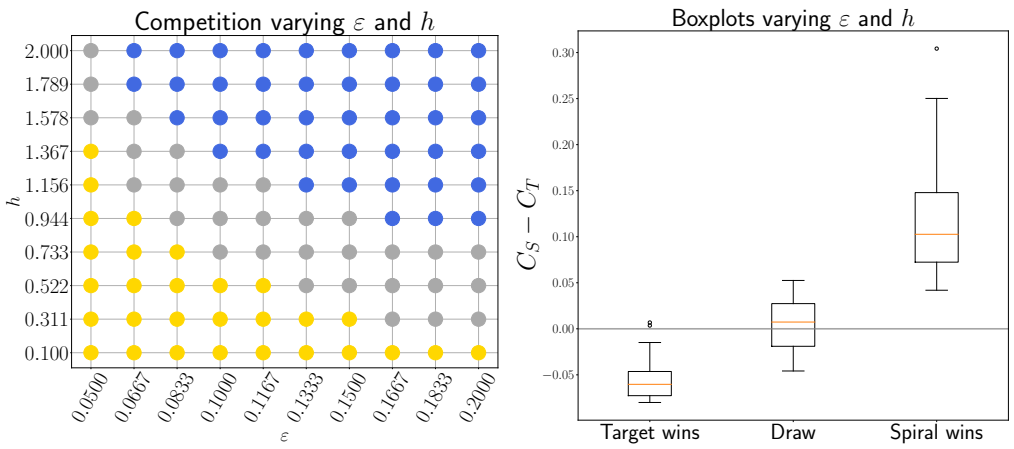

Figure A.11: Competition between spirals and target patterns while varying ε and h of the pacemaker. *Left:* Result of the competition while varying ε and h. The colour of each (ε, h) dot denotes the outcome of the simulation for that pair of parameters: yellow if the spiral has won, gray if both the spiral and target pattern remain (draw), and blue of the target has won. *Right:* Boxplots of the difference in envelope speed of the spirals C_S and the target patterns C_T at all pairs (ε, h), grouped according to the outcome of the competition.

A.4 Experiments

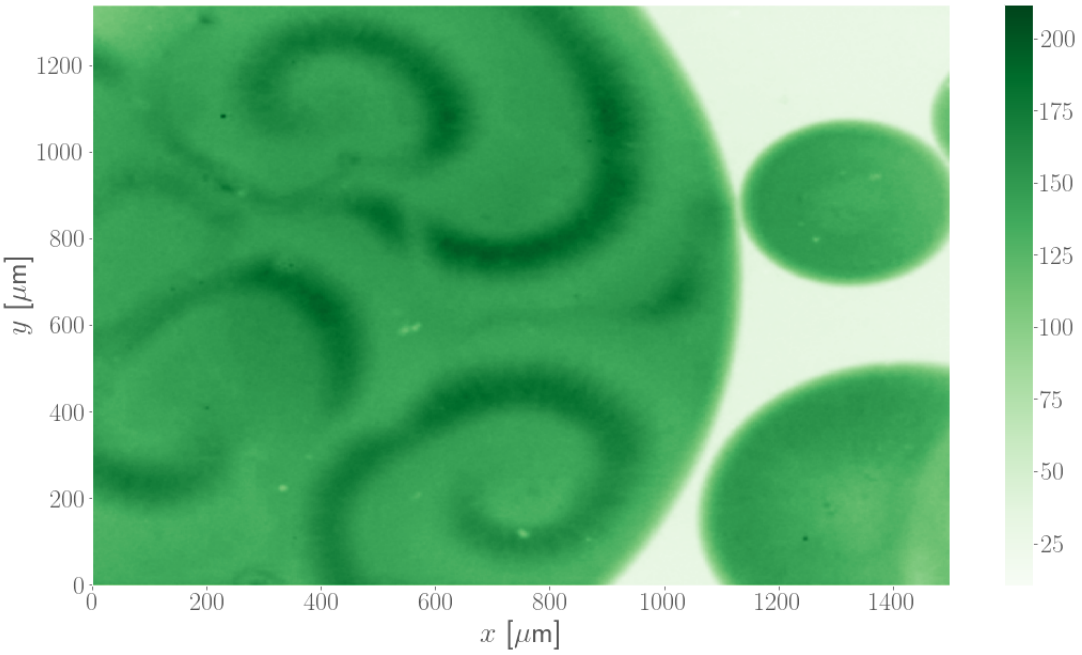

Figure A.12: A snapshot of the experiments performed on *Xenopus laevis* extracts, where spiral waves have been observed.

A.5 Acknowledgements

The computational resources and services used in this work were provided by the VSC (Flemish Supercomputer Center), funded by the Research Foundation Flanders (FWO) and the Flemish Government department EWI.

I would like to thank Lendert Gelens and Daniel Ruiz Reynés for giving me the opportunity to take my first few baby steps into performing independent research, for all our fruitful discussions, their constant support, and for being there whenever I needed their advice.

References

[1] A. Zaikin and A. Zhabotinsky, "Concentration wave propagation in two-dimensional liquid-phase self-oscillating system," *Nature*, vol. 225, no. 5232, pp. 535–537, 1970.

[2] A. L. Belmonte, Q. Ouyang, and J.-M. Flesselles, "Experimental survey of spiral dynamics in the belousov-zhabotinsky reaction," *Journal de Physique II*, vol. 7, no. 10, pp. 1425–1468, 1997.

[3] A. T. Winfree, "Spiral waves of chemical activity," *Science*, vol. 175, no. 4022, pp. 634–636, 1972.

[4] S. Jakubith, H.-H. Rotermund, W. Engel, A. Von Oertzen, and G. Ertl, "Spatiotemporal concentration patterns in a surface reaction: Propagating and standing waves, rotating spirals, and turbulence," *Physical Review Letters*, vol. 65, no. 24, p. 3013, 1990.

[5] J. M. Davidenko, A. V. Pertsov, R. Salomonsz, W. Baxter, and J. Jalife, "Stationary and drifting spiral waves of excitation in isolated cardiac muscle," *Nature*, vol. 355, no. 6358, pp. 349–351, 1992.

[6] J. Lechleiter, S. Girard, E. Peralta, and D. Clapham, "Spiral calcium wave propagation and annihilation in xenopus laevis oocytes," *Science*, vol. 252, no. 5002, pp. 123–126, 1991.

[7] J. Tyson and J. Murray, "Cyclic amp waves during aggregation of dictyostelium amoebae," *Development*, vol. 106, no. 3, pp. 421–426, 1989.

[8] J. J. Tyson, K. A. Alexander, V. Manoranjan, and J. Murray, "Spiral waves of cyclic amp in a model of slime mold aggregation," *Physica D: Nonlinear Phenomena*, vol. 34, no. 1-2, pp. 193–207, 1989.

[9] J. Rombouts and L. Gelens, "Analytical approximations for the speed of pacemaker-generated waves," *Phys. Rev. E*, vol. 104, p. 014220, Jul 2021.

[10] J. Rombouts and L. Gelens, "Synchronizing an oscillatory medium: The speed of pacemaker-generated waves," *Phys. Rev. Research*, vol. 2, p. 043038, Oct 2020.

[11] F. E. Nolet, J. Rombouts, and L. Gelens, "Synchronization in reaction–diffusion systems with multiple pacemakers," *Chaos: An Interdisciplinary Journal of Nonlinear Science*, vol. 30, no. 5, p. 053139, 2020.

[12] F. E. Nolet, A. Vandervelde, A. Vanderbeke, L. Piñeros, J. B. Chang, and L. Gelens, "Nuclei determine the spatial origin of mitotic waves," *Elife*, vol. 9, p. e52868, 2020.

[13] R. FitzHugh, "Mathematical models of threshold phenomena in the nerve membrane," *The bulletin of mathematical biophysics*, vol. 17, no. 4, pp. 257–278, 1955.

[14] J. Nagumo, S. Arimoto, and S. Yoshizawa, "An active pulse transmission line simulating nerve axon," *Proceedings of the IRE*, vol. 50, no. 10, pp. 2061–2070, 1962.

[15] B. van der Pol Jun. D.Sc, "LXXXVIII. On "relaxation-oscillations"," *The London, Edinburgh, and Dublin Philosophical Magazine and Journal of Science*, vol. 2, no. 11, pp. 978–992, 1926.

[16] M.-A. Bray and J. Wikswo, "Use of topological charge to determine filament location and dynamics in a numerical model of scroll wave activity," *IEEE Transactions on Biomedical Engineering*, vol. 49, no. 10, pp. 1086–1093, 2002.

[17] N. D. Mermin, "The topological theory of defects in ordered media," *Rev. Mod. Phys.*, vol. 51, pp. 591–648, Jul 1979.

[18] J. A. Sepulchre and A. Babloyantz, "Motions of spiral waves in oscillatory media and in the presence of obstacles," *Phys. Rev. E*, vol. 48, pp. 187–195, Jul 1993.

[19] L. Arno, J. Quan, N. T. Nguyen, M. Vanmarcke, E. G. Tolkacheva, and H. Dierckx, "A phase defect framework for the analysis of cardiac arrhythmia patterns," *Frontiers in Physiology*, p. 1514, 2021.